Inorg. Chem. **2007**, *46*, 3038–3048

Excited-State Absorption Properties of Platinum(II) Terpyridyl Acetylides

Elena Shikhova,[†] Evgeny O. Danilov,[‡] Solen Kinayyigit,[†] Irina E. Pomestchenko,[†] Alexander D. Tregubov,[†] Frank Camerel,[§] Pascal Retailleau,[||] Raymond Ziessel,*[,§] and Felix N. Castellano*[,†]

Department of Chemistry and Center for Photochemical Sciences, Bowling Green State University, Bowling Green, Ohio 43403, Ohio Laboratory for Kinetic Spectrometry, Bowling Green State University, Bowling Green, Ohio 43403, Laboratoire de Chimie Moléculaire associé au Centre National de la Recherche Scientifique (CNRS), Ecole de Chimie, polyméres, Matériaux (ECPM), 25 rue Becquerel, 67087 Strasbourg Cedex, France, and Laboratoire de Cristallochimie, ICSN−CNRS, Bât 27, 1 avenue de la Terrasse, F-91198 Gif-sur-Yvette, France

Received September 28, 2006

A comprehensive photophysical study is presented which compares the ground- and excited-state properties of four platinum(II) terpyridyl acetylide compounds of the general formula [Pt(^{t}Bu$_3$tpy)(C≡CR)]$^+$, where ^{t}Bu$_3$tpy is 4,4′,4″-tri-*tert*-butyl-2,2′:6′,2″-terpyridine and R is an alkyl or aryl group. [Ru(^{t}Bu$_3$tpy)$_3$]$^{2+}$ and the pivotal synthetic precursor [Pt(^{t}Bu$_3$tpy)Cl]$^+$ were also investigated in the current work. The latter two complexes possess short excited-state lifetimes and were investigated using ultrafast spectrometry while the other four compounds were evaluated using conventional nanosecond transient-absorption spectroscopy. The original intention of this study was to comprehend the nature of the impressive excited-state absorptions that emanate from this class of transition-metal chromophores. Transient-absorbance-difference spectra across the series contain the same salient features, which are modulated only slightly in wavelength and markedly in intensity as a function of the appended acetylide ligand. More intense absorption transients are observed in the arylacetylide structures relative to those bearing an alkylacetylide, consistent with transitions coupled to the π system of the ancillary ligand. Reductive spectroelectrochemical measurements successfully generated the electronic spectrum of the ^{t}Bu$_3$tpy radical anion in all six complexes at room temperature. These measurements confirm that electronic absorptions associated with the ^{t}Bu$_3$tpy radical anion simply do not account for the intense optical transitions observed in the excited state of the Pt(II) chromophores. Transient-trapping experiments using the spectroscopically silent reductive quencher DABCO clearly demonstrate the loss of most transient-absorption features in the acetylide complexes throughout the UV, visible, and near-IR regions following bimolecular excited-state electron transfer, suggesting that these features are strongly tied to the photogenerated hole which is delocalized across the Pt center and the ancillary acetylide ligand.

Introduction

The fundamentally interesting excited-state properties of Pt(II) charge-transfer (CT) complexes based on bipyridyl and terpyridyl acetylides continue to attract the attention of researchers. Indeed, the location of the low-energy absorption band in the visible region with corresponding high quantum yield photoluminescence spanning the visible[1−4] and near-IR (NIR)[1,5] regions facilitates a variety of applications such as dye-sensitized solar cells,[6,7] biosensors,[8] nonlinear transmission,[9] electroluminescent materials,[4] molecular switches,[10]

* To whom correspondence should be addressed. E-mail: castell@bgsu.edu (F.N.C.), ziessel@chimie.u-strasbg.fr (R.Z.).

[†] Department of Chemistry and Center for Photochemical Sciences, Bowling Green State University.

[‡] Ohio Laboratory for Kinetic Spectrometry, Bowling Green State University.

[§] Laboratoire de Chimie Moléculaire associé au Centre National de la Recherche Scientifique.

[||] Laboratoire de Cristallochimie, ICSN−CNRS.

(1) Castellano, F. N.; Pomestchenko, I. E.; Shikhova, E.; Hua, F.; Muro, M. L.; Rajapakse, N. *Coord. Chem. Rev.* **2006**, *250*, 1819−1828.
(2) Hissler, M.; Connick, W. B.; Geiger, D. K.; McGarrah, J. E.; Lipa, D.; Lachicotte, R. J.; Eisenberg, R. *Inorg. Chem.* **2000**, *39*, 447−457.
(3) Whittle, C. E.; Weinstein, J. A.; George, M. W.; Schanze, K. S. *Inorg. Chem.* **2001**, *40*, 4053−4062.
(4) Chan, S.-C.; Chan, M. C. W.; Wang, Y.; Che, C.-M.; Cheung, K.-K.; Zhu, N. *Chem.—Eur. J.* **2001**, *7*, 4180−4190.
(5) Adams, C. J.; Fey, N.; Weinstein, J. A. *Inorg. Chem.* **2006**, *45*, 6105−6107.

10.1021/ic0618652 CCC: $37.00
Published on Web 03/23/2007

and photocatalysis.[11−13] The optical properties of these Pt(II) chromophores are generally tied to the low-lying CT excited states inherent in these molecules. The variability of the CT states to modulation in the electronic properties of the ligands and solvent polarity allows substantial flexibility in tuning the absorption/emission spectra, excited-state lifetimes, emission quantum yields, and transient-absorption (TA) features. The net result is an array of structurally similar complexes with programmable optical properties useful for a variety of applications harnessing their excited-state properties.

Recent theoretical studies using DFT analysis have revealed that the low-lying CT absorptions involve combinations of dπ(Pt) → π* metal-to-ligand CT (MLCT) mixed with π(C≡CR) → π*(tpy) ligand-to-ligand CT (LLCT) transitions.[14−16] Thus, it is this interplay between CT states of different origin that dramatically alters the excited-state properties of the Pt(II) complexes as a function of the electronic properties of the various appended ligands. The excited-state absorption bands exhibit a complexity that likely represents an admixture of CT transitions. The current work seeks to identify the nature of the excited-state absorptions in platinum(II) terpyridyl aryl- and alkylacetylides by correlating a combination of ground-state spectroelectrochemical measurements and reductive-transient-trapping experiments with excited-state-difference spectra. In this work, four platinum(II) terpyridyl acetylide compounds with the general structure $[Pt(^tBu_3tpy)(C{\equiv}CR)]^+$, where $^tBu_3tpy$ is 4,4′,4″-tri-*tert*-butyl-2,2′:6′,2″-terpyridine (R = Ph (phenyl), $SiEt_3$ (triethylsilyl), Tol (tolyl), and ^{t}Bu), are synthesized and structurally characterized. Comprehensive photophysical measurements including the investigation of ground-state absorption, steady-state and time-resolved photoluminescence, electrochemistry, reductive spectroelectrochemistry, and time-resolved excited-state absorption measurements were performed. To support this study, we prepared two model complexes that possess low-energy MLCT transitions and measured their photophysics in parallel with the other molecules. $Ru(^tBu_3tpy)_2(PF_6)_2$[17,18] was selected to best represent a MLCT complex with "pure" MLCT excited states. $[Pt(^tBu_3tpy)Cl]ClO_4$ represents another pivotal model chromophore since it is the closest structural analogue of the compounds under investigation and it is known to possess mainly low-energy MLCT excited states.[19−22]

Experimental Section

1. General Procedures. All synthetic manipulations were performed under an inert and dry argon atmosphere using standard techniques. Anhydrous CH_2Cl_2 (EMD Chemicals) and diisopropylamine (Aldrich) were obtained by distillation over CaH_2. The reagents *p*-tolylacetylene, triethylsilylacetylene, and K_2PtCl_4 were purchased from Fluka and Strem Chemicals, and sodium perchlorate was purchased from Acros. Copper(I) iodide, 4,4′,4″-tri-*tert*-butyl-2,2′:6′,2″-terpyridine, and phenylacetylene were purchased from Aldrich Chemical Co. and used as received. All other reagents and materials from commercial sources were used without further purification. The silica gel used in the chromatographic separations of **1** and **2** was obtained from EM Science (Silica Gel 60, 230−400 mesh). In compounds **4** and **5**, chromatographic purification was conducted using aluminum oxide 90 standardized, deactivated with 6% water by weight. Thin-layer chromatography was performed on aluminum oxide plates coated with a fluorescent indicator. All mixtures of solvents are given in a v/v ratio. The 300 MHz ^{1}H, 400 MHz ^{1}H, and 100 MHz ^{13}C NMR spectra were recorded on Bruker Advance spectrometers at room temperature with perdeuterated solvents, with residual protiated solvent signals providing internal references. All splitting patterns are designated as s (singlet), d (doublet), dd (doublet of doublets), t (triplet), q (quartet), m (multiplet), and br (broad). MALDI mass spectra were measured using a Bruker-Daltonics Omniflex spectrometer. Electrospray mass spectra were acquired using an Agilent MSD analytical apparatus in positive mode; an automatic calibration was used with CH_2Cl_2 as the solvent. FT-IR spectra were recorded on neat liquids or as thin films, prepared with a drop of CH_2Cl_2, and evaporated to dryness on KBr pellets. Elemental analyses were performed by Atlantic Microlab, Norcross, GA. The experimental procedures for each reaction were tested several times and are reported optimized for the best conditions.

2. Syntheses and Structures. Preparations. ***Caution!*** *Perchlorate salts are potential explosion hazards so appropriate precautions should be taken when handling them.* The synthon $[Pt(^tBu_3tpy)Cl]ClO_4$ (**1**) was prepared according to the well-established literature procedure,[21] whereas $[Pt(^tBu_3tpy)Cl]Cl$ was prepared via adaptation of the same reference. ^{1}H (400.129 MHz) NMR: δ 8.94 (s, 2H), 8.91 (d, ^3J = 6.2 Hz, 2H), 8.89 (d, ^4J = 1.8 Hz, 2H), 7.63 (dd, ^3J = 6.2 Hz, ^4J = 1.8 Hz, 2H), 1.63 (s, 9H), 1.52 (s, 18H). MALDI-TOF: *m/z* 1049.67 [$M^+ - ClO_4$].

$[Pt(^tBu_3tpy)(C{\equiv}CPh)]ClO_4$ (2). $[Pt(^tBu_3tpy)Cl]ClO_4$ (0.150 g, 0.205 mmol) was reacted with phenylacetylene (0.06 g, 0.615 mmol) in distilled CH_2Cl_2 (100 mL) in the presence of freshly distilled diisopropylamine (30 mL) and with CuI (0.004 g, 0.022

(6) Islam, A.; Sugihara, H.; Hara, K.; Singh, L. P.; Katoh, R.; Yanagida, M.; Takahashi, Y.; Murata, S.; Arakawa, H. *Inorg. Chem.* **2001**, *40*, 5371−5380.
(7) Geary, E. A. M.; Yellowlees, L. J.; Jack, L. A.; Oswald, I. D. H.; Parsons, S.; Hirata, N.; Durrant, J. R.; Robertson N. *Inorg. Chem.* **2005**, *44*, 242−250.
(8) Wong, K. M.-C.; Tang, W.-S.; Chu, B. W.-K.; Zhu, N.; Yam, V. W.-W. O*rganometallics* **2004**, *23*, 3459−3465.
(9) Guo, F.; Sun, W.; Liu, Y.; Schanze, K. *Inorg. Chem*. **2005**, *44*, 4055−4065.
(10) Yutaka, T.;Mori, I.; Kurihara, M.; Mizutani, J.; Tamai, N.; Kawai, T.; Irie, M.; Nishihara, H. *Inorg. Chem*. **2002**, *41*, 7143−7150.
(11) Zhang, D.; Wu, L.-Z.; Zhou, L.; Han, X.; Yang, Q.-Z.; Zhang, L.-P.; Tung, C.-H. *J. Am. Chem. Soc*. **2004**, *126*, 3440−3441.
(12) Du, P.; Schneider, J.; Jarosz, P.; Eisenberg, R. *J. Am. Chem. Soc.* **2006**, *128*, 7726−7727.
(13) Narayana-Prabhu, R.; Schmehl, R. H. *Inorg. Chem.* **2006**, *45*, 4319−4321.
(14) Zhou, X.; Zhang, H.-X.; Pan, Q.-J.; Xia, B.-H.; Tang, A.-C. *J. Phys. Chem. A* **2005**, *109*, 8809−8818.
(15) Liu, X.-J.; Feng, J.-K.; Meng, J.; Pan, Q.-J.; Ren, A.-M.; Zho, X.; Zhang, H.-X. *Eur. J. Inorg. Chem*. **2005**, 1856−1866.
(16) Hua, F.; Kinayyigit, S.; Cable, J. R.; Castellano, F. N. *Inorg. Chem.* **2006**, *45*, 4304−4306.
(17) Zhou, X.; Ren, A.-M.; Feng, J.-K. *J. Organomet. Chem.* **2005**, *690* (2), 338−347.
(18) Abrahamsson, M.; Jäger, M.; Osterman, T.; Eriksson, L.; Persson, P.; Becker, H. C.; Johansson, O.; Hammarstrom, L. *J. Am. Chem. Soc.* **2006**, *128*, 12616−12617.
(19) Michalec, J. F.; Bejune, S. A.; McMillin. D. R. *Inorg. Chem.* **2000**, *39*, 2708−2709.
(20) Ratilla, E. M. A.; Brothers, H. M., II.; Kostic, N. M. *J. Am. Chem. Soc*. **1987**, *109*, 4592−4599.
(21) Yip, H. K.; Cheng, L. K.; Cheung, K. K.; Che, C. M. *J. Chem. Soc., Dalton Trans.* **1993**, 2933−2938.
(22) Michalec, J. F.; Bejune, S. A.; Cuttell, D. G.; Summerton, G. C.; Gertenbach, J. A.; Field, J. S.; Haines, R. J.; McMillin D. R. *Inorg. Chem*. **2001**, *40*, 2193−2200.

mol) as catalyst. The reaction mixture was stirred under an inert argon atmosphere at room temperature for 17 h while excluding light. Crude product **2** was purified by column chromatography (5 vol % methanol in CH_2Cl_2, SiO_2), yielding a dark-orange crystalline solid in 67% yield.

^{1}H NMR (300 MHz, $CDCl_3$): δ 9.15 (d, 2H, J = 6.0 Hz), 8.44 (s, 2H), 8.37 (d, 2H, J = 2.0 Hz), 7.6 (dd, 2H, J = 6.0 and J = 2.0 Hz), 7.51 (dd, 2H, J = 8.0 and J = 2.0 Hz), 7.31 (m, 3H), 1.59 (s, 9H), 1.51 (s, 18H). MALDI-MS: calculated for $C_{35}H_{40}N_3Pt$, 697.29; found, 697.36. Anal. Calcd for $C_{35}H_{40}ClN_3O_4Pt$: C, 52.69; H, 5.02; N, 5.27. Found: C, 51.50; H, 5.06; N, 5.03.

[Pt(^{t}Bu$_3$tpy)(C≡C^{t}Bu)]ClO$_4$ (3). [Pt(^{t}Bu$_3$tpy)Cl]ClO$_4$ (0.160 g, 0.218 mmol) was reacted with 3,3-dimethyl-1-butyne (0.054 g, 0.654 mmol) in distilled CH_2Cl_2 (150 mL) in the presence of freshly distilled diisopropylamine (50 mL) and with CuI (0.004 g, 0.022 mmol) as catalyst. The reaction mixture was stirred under an inert argon atmosphere at room temperature for 18 h. The volatiles were then removed under reduced pressure. The crude product **3** was recrystallized from chloroform. Yield: 87%. MALDI-MS: calculated for $C_{33}H_{44}N_3Pt$, 677.80; found, 677.38. ^{1}H NMR (300 MHz, $CDCl_3$): δ 9.13 (d, 2H, J = 6.0 Hz), 8.40 (s, 2H), 8.33 (d, 2H, J = 1.8 Hz), 7.64 (dd, 2H, J = 6.0 and J = 2.1 Hz), 1.63 (s, 9H), 1.53 (s, 18H), 1.43 (s, 9H). Anal. Calcd for $C_{33}H_{44}ClN_3O_4Pt$: C, 50.96; H, 5.66; N, 5.41. Found: C, 49.64; H, 5.61; N, 5.23.

[Pt(^{t}Bu$_3$tpy)(C≡CSiEt$_3$)]BF$_4$ (4) and [Pt(^{t}Bu$_3$tpy)(C≡CTol)]BF$_4$ (5). The preparation begins with the dissolution of [(^{t}Bu$_3$tpy)PtCl]Cl (0.200 g, 0.300 mmol) in a mixture of DMF (10 mL) and triethylamine (3 mL), followed by the addition of *p*-tolylacetylene (0.042 g, 0.359 mmol) or triethylsilylacetylene (0.050 g, 0.359 mmol). The solution was degassed by three freeze−pump−thaw cycles to exclude residual oxygen. The addition of CuI (0.0017 g, 0.009 mmol) to the deep-yellow solution resulted in an instantaneous color change to red. After it was stirred at room temperature for 2 days, the deep-red solution was concentrated to roughly 1 mL, filtered over Celite, and then dropped into an aqueous solution (10 mL) containing $NaBF_4$ (1.00 g). The complex was recovered by filtration using standard filter paper and washed with water (3 × 100 mL), and the red solid was dried under high vacuum. Purification was ensured by column chromatography using alumina as a solid support and a gradient of methanol (0−1%) in CH_2Cl_2 as the mobile phase. Ultimate recrystallization by slow evaporation of CH_2Cl_2 from a CH_2Cl_2/cyclohexane solution afforded pure **4** and **5**.

Complex 4: 0.222 g, 90% isolated yield. ^{1}H (400.129 MHz) NMR: δ 9.09 (d, ^3J = 6.2 Hz, 1H), 8.97 (d, ^3J = 6.2 Hz, 1H), 8.49 (s, 2H), 8.44 (d, ^4J = 1.5 Hz, 2H), 7.55 (dd, ^3J = 6.2 Hz, ^4J = 1.5 Hz, 2H), 1.52 (s, 9H), 1.46 (s, 18H), 1.08 (t, ^3J = 8.0 Hz, 9H), 0.66 ppm (q, ^3J = 8.0 Hz, 6H). ^{13}C{^{1}H} (100.612 MHz NMR): δ 168.8, 167.5, 158.8, 153.8, 153.5, 125.1, 123.4, 121.7, 119.6 (C≡C), 105.8 (C≡C), 37.4, 36.4, 30.3, 30.1, 7.9, 5.4. FT-IR (cm^{-1}): 2947, 2920, 2870, 2050 ($\nu_{C\equiv C}$), 1613, 1555, 1478, 1464, 1368, 1258, 1064, 1018, 916. ES-MS: *m*/*z* 735.2 (100%, [M − BF_4]$^+$) in CH_2Cl_2. Anal. Calcd for $C_{35}H_{50}N_3PtSiBF_4$ (M_r = 822.70): C, 51.09; H, 6.13; N, 5.11. Found: C, 50.78; H, 5.94; N, 4.96.

Complex 5: 0.229 g, 96% isolated yield. ^{1}H (400.129 MHz) NMR: δ 9.15 (d, ^3J = 6.0 Hz, 1H), 8.93 (d, ^3J = 6.1 Hz, 1H), 8.44 (s, 2H), 8.42 (m, 2H), 7.61 (dd, ^3J = 6.1 Hz, ^4J = 1.3 Hz, 2H), 7.39 (d of the ABq, J = 8.1 Hz, 2H), 7.13 (d of the ABq, J = 8.1 Hz, 2H), 2.37 (s, 3H), 1.54 (s, 9H), 1.48 (s, 18H). ^{13}C{^{1}H} (100.612 MHz NMR): δ 168.5, 167.8, 159.2, 154.6, 151.2, 136.9, 132.2, 129.2, 125.3, 123.6, 122.5, 104.9, 96.8, 37.8, 36.8, 30.6, 30.5, 21.8. FT-IR (cm^{-1}): 2921, 2853, 2060 ($\nu_{C\equiv C}$), 1606, 1554, 1505, 1463, 1366, 1255, 1046, 1019, 915. ES-MS: *m*/*z* 711.2 (100%, [M − BF_4]$^+$) in CH_2Cl_2. Anal. Calcd for $C_{36}H_{42}N_3PtBF_4$ (M_r = 798.62): C, 54.14; H, 5.30; N, 5.26. Found: C, 54.00; H, 5.12; N, 4.93.

[Ru(^{t}Bu$_3$tpy)$_2$](PF$_6$)$_2$ (6).[23] Ruthenium(III) chloride monohydrate (170 mg, 0.754 mmol) and 680 mg (1.514 mmol) of 4,4′,4″-tri-*tert*-butyl-2,2′:6′,2″-terpyridine were refluxed in 20 mL of anhydrous ethanol for 5 h. After the solution was cooled to room temperature, a concentrated aqueous solution of ammonium hexafluorophosphate was added and the mixture was stirred for 1 h. Upon the addition of 25 mL of water, a dark-red solid precipitated. The solid was collected by vacuum filtration and washed with diethyl ether. The title compound was purified by column chromatography over neutral Al_2O_3 using a gradient elution of toluene/acetonitrile from 1:1 to 1:4. The resulting red powder was obtained by rotary evaporation of the desired fraction. ^{1}H NMR (MeCN-d_3): δ 8.77 (s, 4H), 8.36 (s, 4H), 7.17 (dd, 8H), 1.75 (s, 18H), 1.33 (s, 36H). MALDI-TOF: *m*/*z* 1194.46 [M$^+$], 1049.67 [M$^+$ − PF_6], 904.72 [M$^+$ − 2PF_6].

Single-Crystal X-ray Crystallography. X-ray diffraction data for **4** were recorded from a single, brown (dark-yellow) crystal of dimensions 0.4 mm × 0.2 mm × 0.2 mm, at ambient temperature on an Enraf-Nonius Kappa-CCD diffractometer, using graphite-monochromated Mo Kα (λ = 0.71073 Å) radiation, and performed with the *COLLECT* software.[24] A φ scan with an increment of 1.8° over 183° was performed first and completed by four subsequent ω scans to fill the asymmetric unit. The images were interpreted, and the intensities were integrated using the program *DENZO*.[25] Unique reflections numbering 6421 were obtained from a total of 16 005 measured reflections (R_{int} = 0.029), in the range of *h*, −11 to 11; *k*, −14 to 13; *l*, −19 to 18, with $2\theta_{max}$ = 56.7°. The structure was solved by Patterson methods, expanded to all non-H atoms by the Fourier method (*PATTY*),[26] and refined by full-matrix least-squares on F^2 values using *SHELX-L97*[27] as implemented into *Crystalbuilder-GUI*.[28] In the least-squares refinement, all non-H atoms were refined anisotropically despite the strong dynamic disorder of certain groups (the *tert*-butyl group (C20 > C23), the three ethyl groups attached to Si, the BF_4^- counterion, and the cyclohexane solvent molecule), necessitating geometrical and anisotropic displacement parameter (ADP) restraints. Additionally, the apparent free rotation of the aforementioned *tert*-butyl group was treated by considering two sites per atoms with the occupancy rate refined to $^2/_3$:$^1/_3$. Similarly, the C atoms of the cyclohexane were allowed to take two positions to account for large ADP. H atoms from the pyrrole groups were located on difference Fourier syntheses and then treated like those placed in calculated positions, as riding atoms, with U_{iso} set to 1.2 times that of the attached C atom (1.5 times when it was of a methyl group). Convergence for 541 variable parameters by least-squares refinement on F^2 with w = $1/[\sigma^2(F_o^2) + (0.0591P)^2 + 1.5933P]$, where $P = (F_o^2 + 2F_c^2)/3$

(23) Schubert, U. S.; Eschbaumer, C.; Andres, P.; Hofmeier, H.; Weidl, C. H.; Herdtweck, E.; Dulkeith, E.; Morteani, A.; Hecker, N. E.; Feldmann, J. *Synth. Met.* **2001**, *121*, 1249−1252.

(24) Enraf-Nonius; Delft, The Netherlands, **1997**.

(25) Otwinovski, Z.; Minor, W. *Meth. Enzymology A* **1997**, 307−326.

(26) Beurskens, P. T.; Beurskens, G.; de Gelder, R.; Garcia-Granda, S.; Gould, R. O.; Israel, R. and Smits, J. M. M. The *DIRDIF-99 program system*; Crystallography Laboratory, University of Nijmegen: Nijmegen, The Netherlands, 1999.

(27) Sheldrick, G. M. *SHELX97*; *Program for the Refinement of Crystal Structures from Diffraction Data*; University of Göttingen: Göttingen, Germany, 1997.

(28) Welter, R.; Romang, J. F. *Crystalbuilder-GUI for SHELXL97 on MACOSX*; Louis Pasteur University-Strasbourg: Strasbourg, France, 2002. http://www-chimie.u-strasbg.fr/~decmet/crystalbuilder/crystal-b.html.

for 5480 reflections with $I > 2\sigma(I)$, was reached at $R = 0.0396$ and $R_w = 0.0958$ with a goodness-of-fit value of 1.043. $(\Delta/\sigma)_{max} < 0.001$. The final difference Fourier map was featureless, with maximum positive and negative peaks of +0.692 and −0.843 e $Å^{-3}$, respectively.

Spectroscopic Measurements. UV−vis absorption spectra were measured with a Hewlett-Packard 8453 diode array spectrophotometer, accurate to ±2 nm. Uncorrected steady-state photoluminescence spectra were obtained with a single-photon-counting spectrofluorimeter from Edinburgh Analytical Instruments (FL/FS 900). All photophysical experiments used optically dilute (OD) solutions (absorbance range = 0.09−0.11) prepared in spectroscopic-grade solvents unless otherwise stated. All luminescence samples in 1 cm^2 anaerobic quartz cells (Starna Cells) were deoxygenated with solvent-saturated argon for at least 20 min prior to measurement. Photoluminescence quantum yields were determined using $[Ru(bpy)_3]^{2+}$ in deaerated CH_3CN ($\Phi_{em} = 0.062$)[29] as the quantum counter. Emission lifetimes were measured by means of a nitrogen-pumped broadband dye laser (2−3 nm fwhm) from a PTI instrument (model GL-3300 N_2 laser and model GL-301 dye laser) using the experimental apparatus previously described.[30]

The experimental apparatus for nanosecond TA spectroscopy, operating under the control of LabView, was described earlier.[31] TA spectra and decay kinetics were obtained using the unfocused second or third harmonic provided by a Continuum Surelite I Nd: YAG laser (532 or 355 nm and 5−7 ns fwhm) or a Spectra Physics GCR 230 laser system. The data consisting of a 16- or 32-shot average were analyzed by Origin 6.1 software. All flash photolysis measurements were conducted at the ambient temperature of 22 ± 2 °C. All samples were thoroughly degassed prior to measurements with high-purity argon and kept under an argon atmosphere throughout the experiment. Samples with absorbances of 0.3−0.4 at the excitation wavelength were typically employed in these experiments. To verify the stability of the complexes, UV−vis absorbance spectra were taken before and after all transient experiments. Ultrafast TA spectra and kinetics were obtained using the same apparatus as that described in an earlier publication.[32]

Electrochemistry. Electrochemical measurements were performed in anhydrous DMF solutions with 0.1 M $^nBu_4NClO_4$ (TBAP) or 0.5 M $^nBu_4NPF_6$ (TBAH) as the supporting electrolyte at room temperature, depending on the counterion of the complex. A platinum disk working electrode, a platinum wire auxiliary electrode, and a Ag/AgCl (3M NaCl) reference electrode were used for all the measurements at Bowling Green State University (BGSU). The work at ULP utilized a platinum pseudo-reference electrode. Anhydrous DMF was purchased from Acros or distilled over KOH under reduced pressure, and TBAP and TBAH were recrystallized from ethanol. The solutions were degassed with argon prior to each measurement. The ferrocenium/ferrocene couple ($FeCp_2^{+/0}$) was used as an internal reference for all measurements from both laboratories, and potentials are reported relative to $FeCp_2^{+/0}$, which has $E_{1/2} = +0.55$ V vs aqueous Ag/AgCl with $E_{pa} - E_{pc} = 81$ mV. No *iR* compensation was used. The cyclic- and differential-pulse voltammograms measured at BGSU were recorded with a Bioanalytical Systems Epsilon controller interfaced with a Pentium PC.

UV−vis Spectroelectrochemistry. Spectroelectrochemical measurements were performed in a home-built cell with an optically transparent thin-layer electrode (OTTLE) cell.[33] This home-built capillary apparatus consists of a gold-grid working electrode, a platinum counter electrode, and a Ag/AgCl (3 M NaCl) reference electrode. The optical cell was placed in a plexiglass box with quartz windows and mounted in the HP 8453 such that the light beam passes through the gold-grid working electrode. Solutions were prepared by dissolving 1 mM metal complexes in 0.1 M TBAP/DMF or 0.5 M TBAH/DMF, depending on the counterion of the metal complex. Samples were degassed with argon gas prior to the experiments, and the inert-gas purge was maintained through the mounted box during the measurements to exclude oxygen and water vapor. The ground-state absorption spectrum of the sample contained within the cell at 0 V was used as the spectrophotometer blank. In this configuration, any changes associated with bulk reduction are observed as differences in absorption (ΔA). In all cases, the potentials were maintained at a value 100−200 mV more negative than the first-reduction wave, using the BAS Epsilon system. The electrolysis times ranged between 5 and 9 min. Reductive spectroelectrochemistry yielded clearly observable and stable one-electron-reduction products, whereas the oxidative process performed on the first irreversible wave generated ill-defined, unstable oxidation products at ambient temperature. The original UV−vis spectrum from the $[Pt(^tBu_3tpy)Cl]^+$ complex could not be completely restored after reductive spectroelectrochemistry in CH_2Cl_2 or DMF.

Results and Discussion

Syntheses and Structures. All complexes presented in this study are air-stable solids and are reasonably soluble in both CH_3CN and CH_2Cl_2 (Chart 1). All newly synthesized Pt(II) compounds were structurally characterized by NMR, mass spectrometry, elemental analysis, and FT-IR spectrometry. Dark-yellow prismatic crystals suitable for X-ray analysis were obtained in pure single phase by slow evaporation from a CH_2Cl_2/cyclohexane mixture at room temperature. The asymmetric unit contains one Pt complex, one BF_4^- counteranion, and one disordered cyclohexane molecule in general position. Figure 1 shows the atomic numbering and labeling scheme of the Pt(II) complex. The *tert*-butyl fragment on the central pyridine is disordered, and only the position with a $^2/_3$ occupancy is represented on the ORTEP drawing. The geometry of the Pt center is distorted square planar with Pt−C1′ = 1.967(7) Å, Pt−N1 = 2.020(5) Å, Pt−N2 = 1.962(6) Å, and Pt−N3 = 2.016(6) Å distances and C1′−Pt−N1 = 98.14(26)°, N1−Pt−N2 = 79.95(21)°, N2−Pt−N3 = 81.08(21)°, and N3−Pt−C1′ = 100.82(25)° angles. The whole molecule is planar, and the N2, Pt, C1′, C2′, and Si atoms are all contained in the mean plane of the molecule. Only a slight tilt of 9.6° between the N2−Pt−C1′ and the C1′−C2′−Si axes can be observed, showing that the triethylsilylalkyne fragment did not bind along the pseudo-C_2 geometrical axis of the terpyridine fragment. Additional crystallographic parameters are provided as Supporting Information (Table S1 and Figure S1).

Steady-State Absorption and Photoluminescence Properties. The ground-state absorption spectra of the platinum-

(29) Caspar, J. V.; Meyer, T. J. *J. Am. Chem. Soc.* **1983**, *105*, 5583−5590.
(30) Pomestchenko, I. E.; Luman, C. R.; Hissler, M.; Ziessel, R.; Castellano, F. N. *Inorg. Chem.* **2003**, *42*, 1394−1396.
(31) Pomestchenko, I. E.; Castellano, F. N. *J. Phys. Chem. A* **2004**, *108*, 3485−3495.
(32) Danilov, E. O.; Pomestchenko, I. E.; Kinayyigit, S.; Gentili, P. L.; Hissler, M.; Ziessel, R.; Castellano, F. N. *J. Phys. Chem. A* **2005**, *109*, 2465−2471.
(33) DeAngelis, T. P.; Heineman, W. R. *J. Chem. Educ.* **1976**, *53*, 594−597.

Chart 1

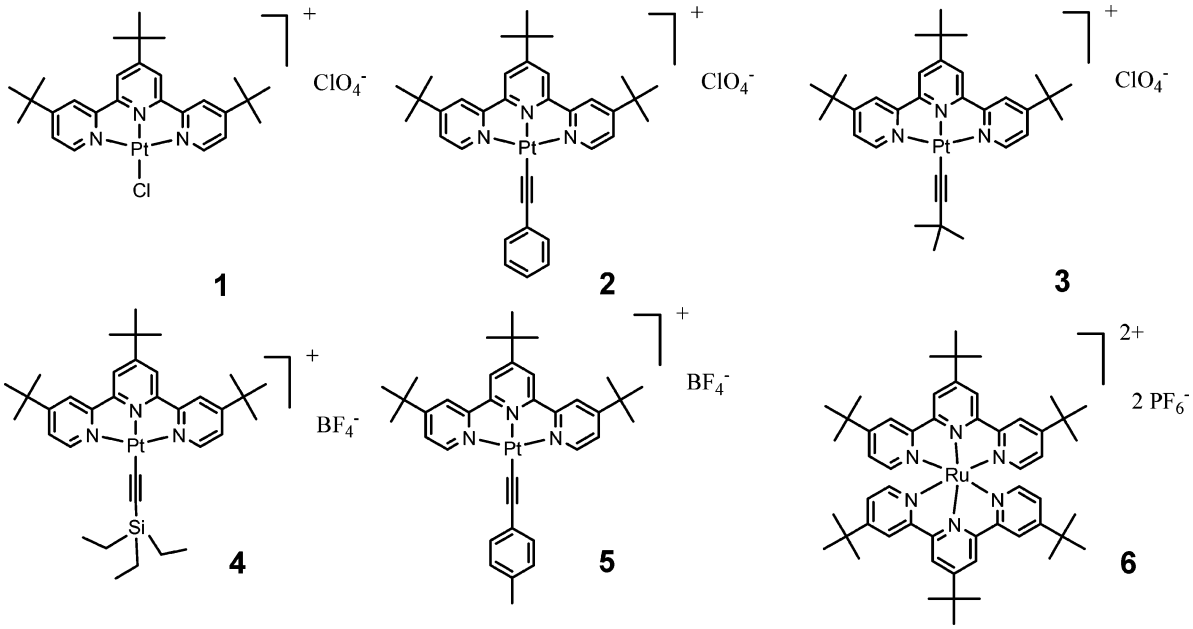

(II) terpyridyl acetylide complexes **1**−**5** were measured in CH_2Cl_2 at room temperature and are presented in Figure 2. In the spectral region between 300 and 600 nm, all investigated complexes display a strong absorption band centered at ∼320 nm and a broad absorption between 360 and 520 nm. For **3** and **4**, this low-energy band is centered at 420−430 nm, whereas in **2** and **5**, the same band apparently consists of two components centered at 410 and 470 nm and 400 and 490 nm, respectively. The intense higher-energy band with extinction coefficients of 15000−30000 M^{-1} cm^{-1} is assigned to ligand-localized $\pi-\pi^*$ transitions.[21] On the basis of the recent results of DFT calculations on similar compounds,[14−16] the broad absorption bands at lower energy with extinction coefficients of ∼3200−5000 M^{-1} cm^{-1} are most likely composed of overlapping MLCT and LLCT transitions. Previous experimental and theoretical work has revealed that the nature of the substituents on the terpyridyl and acetylide ligands dramatically affects the lowest-energy excited states of the Pt(II) complexes by modulating the HOMO−LUMO energy gap. The two major controlling influences are the σ-donating ability of the substituents and the extent of conjugation in the acetylide group. Increasing the σ-donating ability of the acetylide causes destabilization of the HOMO and a concomitant decrease of ΔE, shifting the low-energy absorption band to the red region. This is the primary reason why the low-energy band of **3** is red-shifted when directly compared to the absorption spectrum of **4**. Extending the conjugation in the acetylide group provides additional low-energy electronic states which then participate in LLCT transitions. As a result, the low-energy CT bands in complexes **2** and **5** are substantially broadened relative to the corresponding absorptions in compounds **3** and **4**. Since a more substantial contribution of acetylide electron density to the HOMO increases the role of the LLCT transitions, it may be possible to alter the character of the lowest-energy transition from mixed to pure MLCT or pure LLCT by regulating these factors.

The photoluminescence spectra of **2**−**5** collected at room

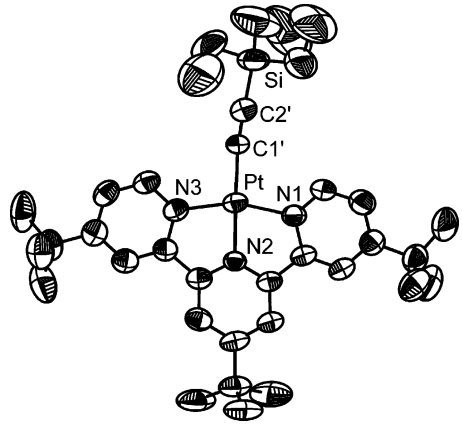

Figure 1. ORTEP drawing of **4** with thermal ellipsoids drawn at the 50% probability level.

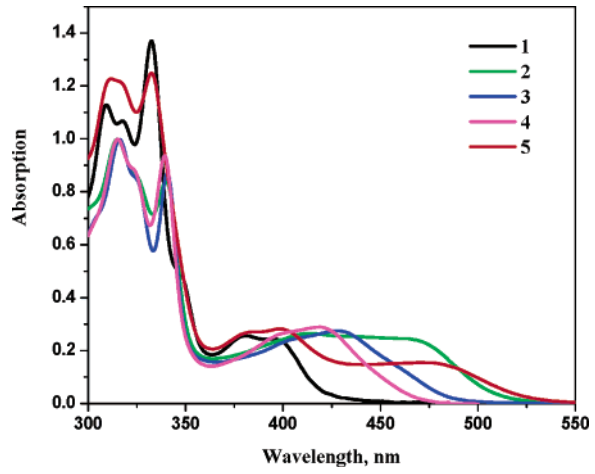

Figure 2. Normalized room-temperature absorption spectra of the complexes **1** (black line), **2** (green line), **3** (blue line), **4** (magenta line), and **5** (red line) in CH_2Cl_2.

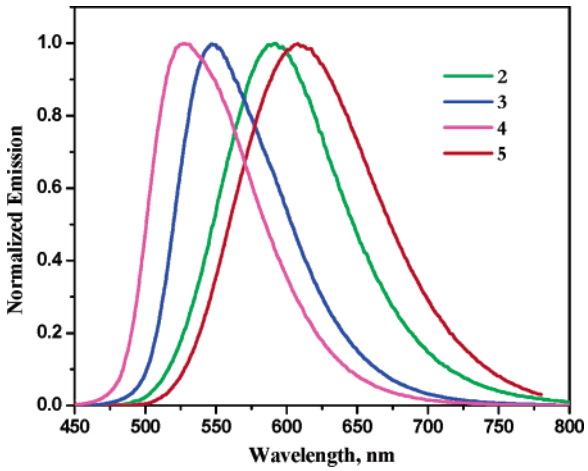

Figure 3. Normalized room-temperature emission spectra of the complexes **2** (green line), **3** (blue line), **4** (magenta line), and **5** (red line) in deaerated CH_2Cl_2.

temperature in degassed CH_2Cl_2 solutions measured under OD conditions are shown in Figure 3. Upon photoexcitation into the CT transitions, **2**−**5** exhibit broad structureless photoluminescence over the range of 475−800 nm. [Pt(^{t}Bu$_3$-tpy)Cl]ClO_4, complex **1**, is completely nonluminescent in fluid solution at 298 K,[22] resulting from radiationless decay of the excited state via a low-lying metal-centered ligand field state.[34] On the basis of the large Stokes shifts, relatively long lifetimes (1−3 μs), and dynamic quenching by air (O_2), the emission can be assigned as triplet charge transfer in nature in all the Pt(II) molecules. All emission spectra were completely invariant to the excitation wavelength in each instance. The emission maximum in **5** is 20 nm red-shifted relative to that of **2**, illustrating the stronger σ-donating ability of a *p*-tolylacetylide versus the phenylacetylide substituent, confirming that the acetylide electronic structure plays a significant role in determining the position of the HOMO in these molecules. The same reasoning can be used to explain the red shift of the emission maximum in **3** compared with that of **4**; however, the stabilizing nature (electron withdrawing) of the $SiEt_3$ moiety is predominately responsible for the green emission displayed by **4**.[35] As mentioned above, expansion of the π conjugation in the acetylide ligands also aids in decreasing the energy gap, and therefore, the emission spectra of complexes **2** and **5** are red-shifted compared with those of complexes **3** and **4**. The room-temperature absorption and photoluminescence properties of the investigated complexes are collected in Table 1, along with their calculated values of k_r and k_{nr}. An interesting observation is that the value of k_{nr} increases by a factor of 3.5 between **2** and **5**. If one correlates k_{nr} differences between Pt(dbbpy)-(C≡CPh)$_2$ and Pt(dbbpy)(C≡CTol)$_2$ using literature data in the same solvent,[3,31] an increase of 2.2-fold is revealed, similar to the present case but slightly attenuated. These somewhat surprising differences in k_{nr} are not obvious based on the structural differences between phenyl- and tolylacetylide nor are they anticipated based on energy-gap considerations. Therefore, they must have their origin in subtle electronic structure differences, particularly in how these acetylide ligands interact and mix with the metal-based orbitals. Since these electronic differences are not revealed in electrochemistry experiments (see below), we believe that this problem deserves a detailed theoretical investigation.

Table 1. Photophysical Properties of the Platinum(II) Terpyridyl Acetylide Complexes **2**−**5** Measured at Room Temperature in Argon-Saturated CH_2Cl_2

compound	λ_{abs}, nm (ϵ, M^{-1} cm^{-1})	λ_{em}, nm	$\tau_{0\ em}$,[a] μs	Φ_{em}[b]	k_r, s^{-1} [c]	k_{nr}, s^{-1} [d]
2	315, 340, 411 (4750), 458 (4380)	592	2.9	0.10	3.4×10^4	3.1×10^5
3	315 (9547), 341 (8804), 406 (3224), 426 (3873)	548	2.2	0.17	7.7×10^4	3.8×10^5
4	315, 339, 400 (4539), 424 (4781)	528	1.9	0.08	4.2×10^4	4.8×10^5
5	312, 332, 380 (3913), 398 (4136), 463 (2302)	608	0.85	0.035	4.1×10^4	1.1×10^6

[a] Emission intensity decay lifetime, ±5%. [b]Quantum yield of photoluminescence measured relative to $[Ru(bpy)_3](PF_6)_2$ ($\Phi_{em} = 0.062$)[29] in CH_3CN. [c] Radiative decay rate, calculated by $k_r = \Phi_{em}/\tau_{em}$. [d] Nonradiative decay rate, calculated by $k_{nr} = (1 - \Phi_{em})/\tau_{em}$; it is assumed that the emitting excited state is produced with unit efficiency.

Table 2. Cyclic Voltammetry Data at Room Temperature in DMF[a]

complex	$E_{1/2}$/V vs $FeCp_2^{+/0}$ [g]	
1[b]	+0.45[e]	−1.34, −1.91, −2.66 (DPV)[h]
2[b]	>+1.15	−1.38, −1.92
3[b]	>+1.15	−1.43, −1.99
4[d]	>+1.17	−1.34, −1.91
5[d]	>+1.14	−1.35, −1.93
6[c,f]	+0.65	−1.78, −2.02

[a] All measurements made at room temperature using a scan rate of 200 mV/s unless otherwise indicated. [b] Measured in 0.1 M TBAP. [c] Measured in 0.5 M TBAH. [d] Measured in 0.1 M TBAH. [e] E_{pa} refers to the anodic peak potential for the irreversible oxidation waves. [f] $E_{1/2}$ oxidation potential; cyclic voltammogram was completely reversible. [g] $E_{1/2} = (E_{pa} + E_{pc})/2$; E_{pa} and E_{pc} are anodic and cathodic peak potentials, respectively. [h] Reduction measured using differential-pulse voltammetry.

Electrochemistry and Spectroelectrochemistry. The electrochemical data of the compounds in this study are summarized in Table 2. All the complexes show two reversible couples at ca. −1.35 and −1.92 V. For [Pt(^{t}Bu$_3$-tpy)Cl]ClO_4, a third reduction at −2.66 V was observed by differential-pulse voltammetry (DPV). The relative insensitivity of the reduction potentials toward the nature of the acetylide ligand suggests that these reductions arise mainly from the terpyridine reductions with some mixing of Pt(II) metal character.[36,37] No oxidation process could be observed

(34) McMillin, D. R.; Moore, J. J. *Coord. Chem. Rev.* **2002**, *229*, 113−121.
(35) Hua, F.; Kinayyigit, S.; Cable, J. R.; Castellano, F. N. *Inorg. Chem.* **2005**, *44*, 471−473.
(36) Hill, M. G.; Bailey, J. A.; Miskowski, V. M.; Gray, H. B. *Inorg. Chem.* **1996**, *35*, 4585−4590.
(37) Crites, D. K.; Cunningham, C. T.; McMillin, D. R. *Inorg. Chim. Acta* **1998**, *273*, 346−353.

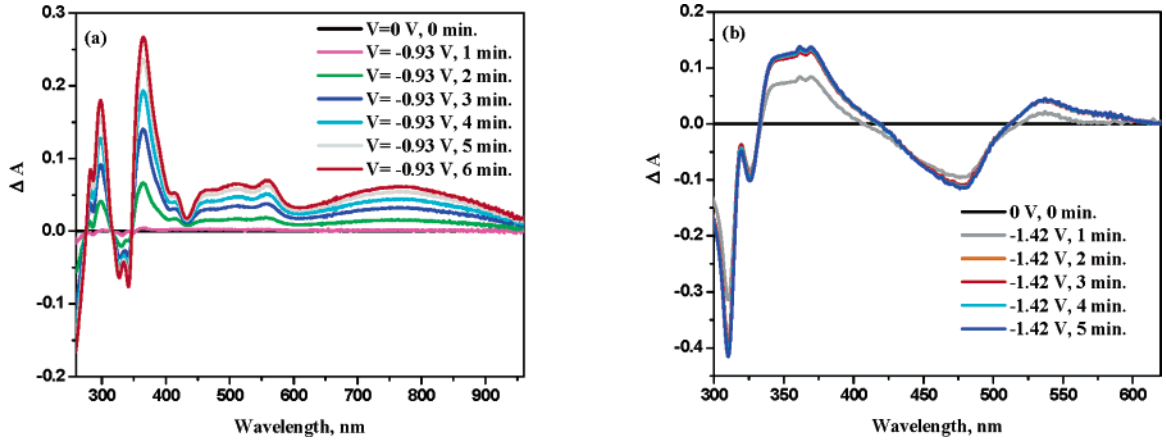

Figure 4. UV−vis absorption spectral changes accompanying the reductive-controlled-potential electrolysis as a function of time at room temperature: (a) 1 mM of **2** at −0.93 V vs Ag/AgCl in 0.1 M TBAP/DMF; (b) 1 mM of **6** at −1.42 V vs Ag/AgCl in 0.5 M TBAH/DMF.

beyond +1.15 V due to the limited potential range of the TBAP/DMF electrolyte solution. When the potential range of the supporting electrolyte solution permits, an irreversible anodic wave is observed, which is assigned to a HOMO-centered oxidation, with most substantial contributions coming from the oxidation of Pt(II) to Pt(III).[38,39]

Spectroelectrochemical measurements were performed on compounds **1**−**3** and **6**. Since the data for **1**−**3** are quite similar, only the data generated on compounds **2** and **6** are presented in Figure 4 for illustrative purposes. The remaining reductive spectroelectrochemical data are provided as Supporting Information (Figures S2−S5). Compounds **1**−**3** are unstable toward oxidative-controlled-potential electrolysis, but all compounds are stable with regards to reductive spectroelectrochemistry. In the case of **6**, which possesses no acetylide ligands but only the ^{t}Bu$_3$tpy ligand, the $\pi-\pi^*$ transitions of the ^{t}Bu$_3$tpy ligand attenuate upon one-electron reduction of the complex while two new absorption bands develop at 361 and 537 nm, corresponding to intraligand transitions of the ^{t}Bu$_3$tpy radical anion (^{t}Bu$_3$tpy$^{\bullet -}$), similar to the absorptions observed in the electrochemically generated one-electron-reduced ruthenium(II) terpyridyl and platinum(II) bipyridyl complexes previously studied.[40−44] UV−vis spectroelectrochemical reduction of 1 mM **1** was performed in both CH_2Cl_2 (Figure S2a) and DMF (Figure S2b) to better correlate these data with ultrafast TA measurements (see below). In DMF, as the potential is stepped just past the first reduction, the absorption bands at 256, 329, and 344 nm and the CT band between 360 and 400 nm disappear while new absorptions appear at 362, 560, and 770 nm, indicative of the formation of ^{t}Bu$_3$tpy$^{\bullet -}$. There is also a shoulder to the red side of the 362 nm band at 418 nm. This reduction process is somewhat reversible on the spectroelectrochemical time scale (minutes), and the initial absorption spectrum is partially (∼70%) regenerated after removal of the negative bias on the OTTLE cell. Similar data were obtained using the CH_2Cl_2 solvent except that the lower-energy visible band shifts to the red (421 nm), becoming better defined relative to the similar feature observed as a shoulder on the 362 nm band in DMF. Since the electrolysis is not completely reversible in either solvent, comparison to the TA-difference spectrum will not be definitive. Controlled-potential electrolysis of **2** and **3** shows behavior similar to that of **1**. In both absorption-difference spectra, there is a decrease in the transitions around 327 and 341 nm that originate from the ^{t}Bu$_3$tpy ligand. New bands are observed for both reduced complexes at 362, 562, and 763 nm in **2** and at 368, 568, and 777 nm for **3**, which result from one-electron reduction of the ^{t}Bu$_3$tpy ligand, which is essentially the same trend as that seen in the spectroelectrochemical data of model compound **1**. The major difference between the spectra generated upon the reduction of the model compound **1** and those of the platinum(II) terpyridyl acetylide complexes is that the new bands produced in the region of 425−600 nm are more structured in the acetylide complexes. In the acetylide complexes, more complete regeneration of the original UV−vis spectrum was observed in each case following electrolysis.

The second reduction of **2** has been studied spectroelectrochemically and compared to the first-reduction-product absorption-difference spectrum. With the increase of voltage beyond the second-reduction wave, a decrease and slight red shift in the absorption of a newly formed band at 365 nm during the first reduction is observed. Another band originally resolved between 670 and 1000 nm during the first-electron addition to the complex also starts decreasing during the second-reduction process. On the other hand, the broad band in the region of 450−600 nm loses its structure but grows stronger with a shift to the red upon the second reduction. Given the fact that the ^{t}Bu$_3$ groups likely suppress dimerization[36] in solution at room temperature, we believe that this second-reduction process does indeed represent double reduction of the ^{t}Bu$_3$tpy ligand,[45,46] which is not accessible optically.

(38) Blanton, C. B.; Murtaza, Z.; Shaver, R. J.; Rillema, D. P. *Inorg. Chem.* **1992**, *31*, 3230−3235.
(39) von Zelewsky, A.; Gremaud, G. *Helv. Chim. Acta* **1988**, *71*, 1108−1115.
(40) Berger, R. M.; McMillin, D. R. *Inorg. Chem.* **1988**, *27*, 4245−4249.
(41) Klein, A.; Kaim, W. *Organometallics* **1995**, *14*, 1176−1186.
(42) Collison, D.; Mabbs, F. E.; McImnes, E. J. L.; Taylor, K. J.; Welch, A. J.; Yellowlees, L. J. *J. Chem. Soc., Dalton Trans.* **1996**, 329−334.
(43) Heath, G. A.; Yellowlees, L. J.; Braterman, P. S. *J. Chem. Soc., Chem. Commun.* **1981**, 287−289.
(44) Weinstein, J. A.; Zheligovskaya, N. N.; Mel'nikov, M. Y.; Hartl, F. *J. Chem. Soc., Dalton. Trans.* **1998**, 2459−2466.

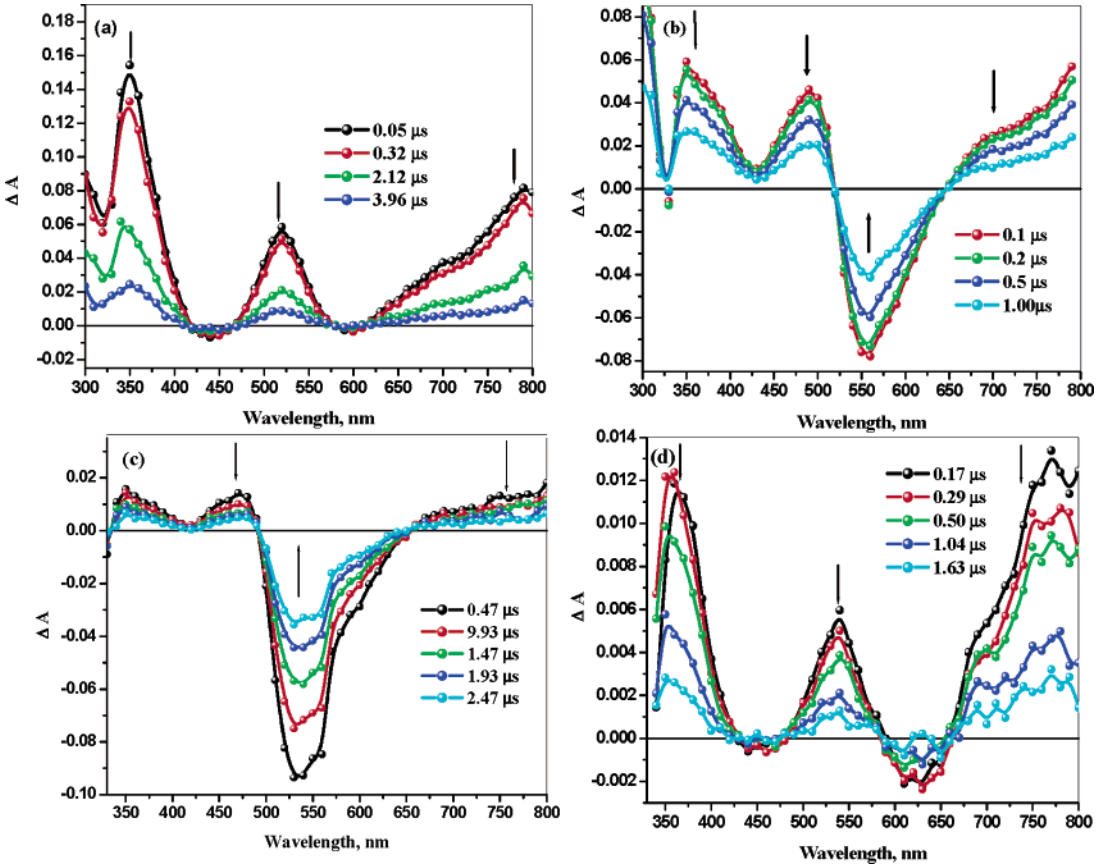

Figure 5. TA-difference spectra of (a) **2**, (b) **3**, (c) **4**, and (d) **5** measured in CH_2Cl_2 following a 3 mJ, 355 nm laser pulse. The delay times are specified on each graph. The strong bleaching signals between 500 and 600 nm in b and c are photoluminescence artifacts.

Nanosecond UV−vis TA Spectroscopy. Nanosecond TA measurements were performed on **2**−**5** at room temperature in CH_2Cl_2 purged with an argon stream. The TA-difference spectra determined at different delay times after a 355 nm laser pulse are shown in Figure 5. No transient absorptions from [Pt(^{t}Bu$_3$tpy)Cl]ClO$_4$ were observed in the nanosecond experiments due to its short excited-state lifetime ($\tau \leq 1$ ns, vide infra). The TA spectra for all compounds look similar, with two distinct positive absorption peaks near 320 nm and between 500 and 550 nm, a negative signal centered around the emission maxima of the compounds (592 (**2**), 548 (**3**), 528 (**4**), and 608 nm (**5**)) corresponding to the emission from the triplet CT state, and a very broad positive absorption band which extends into the NIR region (690−800 nm), continuing beyond our current detection range. In the valley between the first two bands on the blue-green side of the transient spectra, the signal minimizes, going negative in compounds **2** and **5**. This spectral region is associated with the maxima of the respective low-energy ground-state absorption. Accordingly, the shapes of the transient spectra in this region are determined by a combination of positive excited-state absorptions and negative ground-state absorption bleaching bands. Interpretation is complicated by the fact that in all cases the data result from a combination of the transient signals of opposite signs. For all compounds, both positive and negative components of the transient signal decay monoexponentially, producing very clear isosbestic points around 420, 470, 580, and 610 nm (**2**), 525 and 655 nm (**3**), 500 and 650 nm (**4**), and 430, 475, 580, and 665 nm (**5**). No difference in lifetimes was observed as a function of the detection wavelength, regardless of whether they correspond to TA or bleaching.

Upon laser excitation, the platinum(II) terpyridyl acetylide complexes undergo electron density redistribution toward the terpyridyl moiety. It has therefore been common to assign the positive absorptions throughout the visible and NIR regions to terpyridyl radical anion formation resulting from MLCT.[11,47] However, the excited-state absorption spectra comprise all elements contributing to the CT state, the terpyridyl ligand with increased electron density, and also a "hole" with decreased electron density delocalized over the Pt center and acetylide framework. To isolate the contribution of the terpyridyl radical anion to the TA signals, we performed a reductive quenching experiment with the idea to restore the electron density on the platinum−acetylide moiety lost in the act of photoexcitation. A transient spectrum taken after reductive quenching would therefore reflect a more distilled contribution from the terpyridyl radical anion. It is well-known that aliphatic amines serve as good

(45) Mamo, A.; Stefio, I.; Parisi, M. F.; Credi, A.; Venturi, M.; Di, Pietro, C.; Campagna, S. *Inorg. Chem.* **1997**, *36*, 5947−5950.
(46) Bassani, D. M.; Lehn, J. M.; Serroni, S.; Puntoriero, F.; Campagna, S. *Chem.−Eur. J.* **2003**, *9*, 5936−5946.
(47) Chakraborty, S.; Wadas, T. J.; Hester, H.; Flaschenreim, C.; Schmehl, R.; Eisenberg, R. *Inorg. Chem.* **2005**, *44*, 6284−6293.

Scheme 1. Charge-Separation and Charge-Recombination Electron-Transfer Reactions in the Pt/DABCO System[a]

$$[Pt(II)(tBu_3tpy)(CCR)]Y \xrightarrow{h\nu} {}^{1,3}\left[[Pt(III)(tBu_3\dot{tpy}^{-})(CCR)]Y\right]^{*} \xrightarrow{DABCO} [Pt(II)(tBu_3\dot{tpy}^{-})(CCR)]Y + D\dot{A}BCO^{+}$$

$$[Pt(II)(tBu_3\dot{tpy}^{-})(CCR)]Y + D\dot{A}BCO^{+} \longrightarrow [Pt(II)(tBu_3tpy)(CCR)]Y + DABCO$$

[a] Represented with the hole localized on the metal center to simplify the presentation.

Table 3. Rate Constants for the Reductive Quenching of the Platinum(II) Terpyridyl Acetylide Complexes with DABCO, Measured in CH_2Cl_2

Pt(II) complex	k_q (10^9 M^{-1} s^{-1})
2	9.6 ± 0.6
3	8.9 ± 0.2
4	7.3 ± 0.5
5	6.2 ± 0.2

intermolecular reductive quenchers of transition-metal complexes,[48−51] so we focused our attention on this class of quenchers. In our experiments we selected 1,4-diazabicyclo-[2.2.2]octane (DABCO) as the quencher, since the one-electron-oxidation product does not have appreciable absorption in the visible and NIR regions.[50] Photoluminescence-lifetime quenching experiments with DABCO showed that the amine successfully suppresses emission of the investigated complexes through a dynamic quenching mechanism. Degassed solutions of **2**−**5** containing varying concentrations of DABCO were excited at wavelengths corresponding to the CT band. The triplet decay following excitation in the CT region was then monitored at wavelengths where the complexes produced maximum emissions. The luminescence lifetimes of the platinum(II) terpyridyl acetylide complexes were well modeled using single exponentials over the entire range of DABCO concentrations (0.03−0.5 M), demonstrating that the bimolecular quenching cleanly obeys pseudo-first-order kinetics. The values of the rate constants for the lifetime quenching of the triplet state of the platinum(II) terpyridyl acetylide complexes were calculated using the Stern−Volmer equation and are presented in Table 3. These constants approach the value expected for a diffusion-controlled reaction (1.6×10^{10} M^{-1} s^{-1} in CH_2Cl_2),[52] and no significant deviations from linear Stern−Volmer behavior were observed over the entire quencher concentration range (Supporting Information, Figure S6). The steps of the photoinduced electron-transfer reaction from DABCO as an electron donor to the triplet state of the Pt(II) complexes are shown in Scheme 1. Upon 355 nm laser excitation, all compounds undergo a rapid CT leading to the quenching and reduction of the Pt(II) complex to form $DABCO^{\bullet+}$ and $[Pt(^tBu_3tpy^{\bullet-})(C{\equiv}CR)]^+$. $DABCO^{\bullet+}$ can be considered a spectroscopically silent reagent since its absorption in the visible region (at 450 nm) has a low extinction coefficient (<1500 M^{-1} cm^{-1}).[53] Consequently, the resulting excited-state-difference spectra should reveal characteristic absorption features of the $^tBu_3tpy$ radical anion while suppressing all other contributions from the CT excited state. Time-resolved TA-difference spectra for complexes **2**−**5** were measured in CH_2Cl_2 in the presence of DABCO (3 mM solution). Immediately after the laser pulse, the transient spectra in the presence of DABCO resemble those in the absence of the quencher (Figure 5). In a few tens of nanoseconds, the spectra substantially change as a result of reductive quenching in the presence of large quencher concentration. The triplet-state lifetimes become much shorter, dropping below the instrument response time in the cases of **4** and **5** (Figure S7). At delay times 3-fold longer than the quenched lifetime, one can ignore the contributions to the transient spectra from the triplet CT excited state. The spectra taken after this time delay (Figure 6) demonstrate that only one distinct peak remains at high energy between 350 and 360 nm. Since the only common structural feature in the studied compounds is the $^tBu_3tpy$ ligand, we assign the band at 350−360 nm to the $^tBu_3tpy$ radical anion. The long-lived component of the kinetic traces in the presence of the quencher accounts for the charge-recombination reaction between $[Pt^{II}(^tBu_3tpy^{\bullet-})(C{\equiv}CR)]^+$ and $DABCO^{\bullet+}$, which presumably follows diffusion-controlled second-order equal-concentration kinetics ($\sim 10^9-10^{10}$ M^{-1} s^{-1}). We did not investigate the charge-recombination kinetics since this aspect is far beyond the scope of this work. The most important facet of the reductive quenching data is that in all cases the excited-state-difference spectra of the platinum-(II) terpyridyl acetylide complexes is not solely attributable to the $^tBu_3tpy^{\bullet-}$ species. Therefore, the predominately absorbing components in the excited state result from transitions within the photogenerated hole or those associated with the intramolecular charge separated species, i.e., MLCT or LLCT transients.

Ultrafast TA Spectroscopy. A spectral signature of untainted $^tBu_3tpy^{\bullet-}$ is also expected to appear in TA spectra of model compounds whose structure exclusively produces only low-energy MLCT transitions. A good example of this motif is the Ru(II) complex **6**[17,18] or, more appropriately, the Pt(II) complex **1**. Since no transients can be observed at room temperature on the nanosecond time scale for these compounds, ultrafast TA spectra were measured in both instances. Figure 7 displays the TA spectral evolution recorded at different delay times for **6** in CH_2Cl_2 after a 100 fs, 490 nm excitation by laser pulse. The transient spectrum is characterized by an intense positive absorption near 360 nm, ground-state absorption bleaching centered around 485 nm, and a weak broad TA band between 550 and 750 nm. The bleaching corresponds to the lowest-energy ground-state absorption band assigned to the MLCT transition, and the sharp feature at 490 nm is simply due to the scattering from the optical pump pulse. The transient spectrum decays with

(48) Pischel, U.; Xiang, Z.; Hellrung, B.; Haselbach, E.; Muller, P. A.; Nau, W. M. *J. Am. Chem. Soc.* **2000**, *122*, 2027−2034.
(49) Turro, N. J.; Engel, R. *J. Am. Chem. Soc.* **1969**, *91*, 7113−7121.
(50) Lishan, D. J.; Hammond, G. S.; Yee, A. W. *J. Phys. Chem.* **1981**, *85*, 3435−3440.
(51) Inbar, S.; Linschitz, H.; Cohen, S. *J. Am. Chem. Soc.* **1981**, *103*, 1048−1054.
(52) Murov, S. L.; Carmichael, I.; Hug, G. L. *Handbook of Photochemistry*, 2nd ed.; Marcel Dekker: New York, 1993.
(53) Shida, T.; Nosaka, Y.; Kato, T. *J. Phys. Chem.* **1978**, *82*, 695−698.

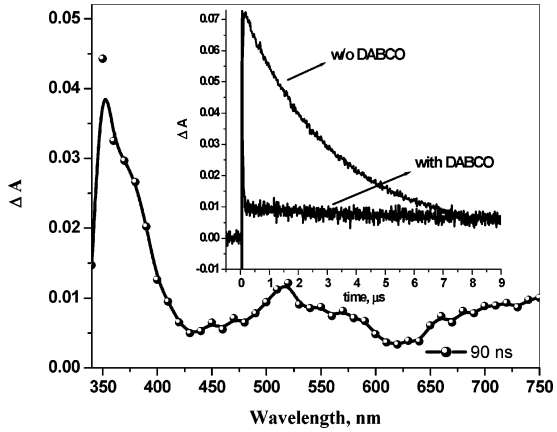

Figure 6. TA spectra and time-resolved-absorption kinetics (monitored at 370 nm) of **2** in the presence of DABCO in CH_2Cl_2; $\lambda_{exc} = 355$ nm, 3 mJ/pulse.

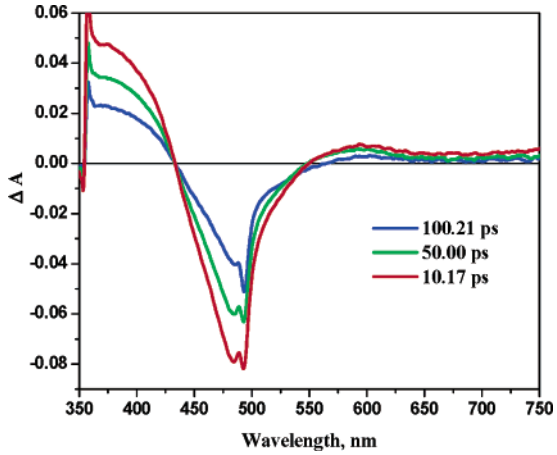

Figure 7. Excited-state absorption-difference spectra of **6** in CH_2Cl_2, excited at 490 nm (~100 fs fwhm), with delay times specified on the graph. The sharp feature at 490 nm superimposed on the low-energy side of the ground-state bleaching present at all delay times is an artifact from pump beam scattering.

first-order kinetics, with a lifetime of 115 ps at all examined probe wavelengths either corresponding to positive TA or bleaching features. The ultrafast TA-difference spectrum resembles the absorption-difference spectrum of the electrochemically obtained terpyridyl radical anion (Figure 4b). Even the asymmetric, shark-fin shape of the ground-state absorption bleaching is retained. On the basis of the spectroelectrochemical data and previous literature reports, we assign the positive TA to the electronic transitions of the one-electron-reduced ^{t}Bu$_3$tpy ligand.[36,39,40]

The TA spectrum for **1** in CH_2Cl_2 following a 100 fs excitation laser pulse at 340 nm is shown in Figure 8. The transient spectrum shows positive absorptions around 360, 470, and 600 nm. The transient spectrum of **1** decays monoexponentially with $\tau = 650 \pm 50$ ps at all examined wavelengths, and the features likely correspond to the triplet MLCT excited state. One interesting observation is that the dip in the spectrum centered at 520 nm may be due to stimulated emission from **1**. We are currently investigating how the Pt(II) metal center may facilitate such a process by permitting strong mixing of the singlet and triplet CT manifolds. As in the case of **6**, one would anticipate that the

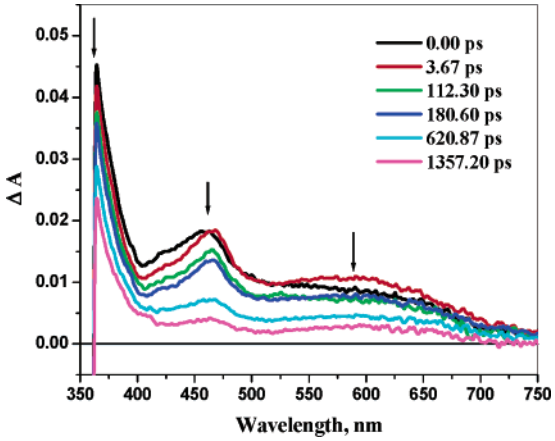

Figure 8. Excited-state absorption-difference spectra of **1** in CH_2Cl_2, excited at 340 nm (~100 fs fwhm), with delay times specified on the graph.

TA corresponding to ^{t}Bu$_3$tpy$^{\bullet -}$ formed upon photoexcitation find their match in reductive spectroelectrochemistry. As we have seen above, the electrochemical-difference spectra correlate remarkably well with the ultrafast TA spectra for **6**. This, however, is not the case for Pt(II) compounds. Whereas the ultrafast TA spectrum of **1** presented in Figure 8 has a shape similar to that of the reductive spectroelectrochemical data for the complex (Supporting Information, Figure S2), the two major band positions in the visible region are significantly shifted from the corresponding features observed in the ground-state one-electron-reduced species. At the moment, we do not know the origin of this discrepancy but speculate that some of the difference may simply result from attempting to correlate the excited-state-difference spectrum to that of an ill-defined ground-state reduced species. In addition, this experiment does not account for any transients associated with excited-state transitions between species generated after the laser pulse. These issues, combined with the fact that we cannot perform the complementary oxidative electrolysis experiment, only permit us to conclude that the excited-state spectrum of **1** cannot be definitively traced to solely ^{t}Bu$_3$tpy radical anion components. Although the complete origins of the transient-difference spectrum in **1** remain under investigation at this point, those measured in **2**−**5** clearly indicate that the large excited-state absorptions associated with these structures are not simply composed of reduced-ligand- and oxidized-metal-center constituents.

Conclusions

Several [Pt(^{t}Bu$_3$tpy)(C≡CR)]$^+$ complexes (**2**−**5**) with substituted acetylide ligands have been synthesized along with the relevant model compounds **1** and **6**. Bright photoluminescence and long-lived excited states (up to 3 μs) of the whole series of compounds make them attractive for numerous applications. The electronic nature of the acetylide ligands is largely responsible for the absorption/emission characteristics of these complexes and can be used to readily modulate photophysical properties. Not surprisingly, the reductive spectroelectrochemical data for all the Pt(II) complexes are almost identical, since the ^{t}Bu$_3$tpy radical anion is the primary absorbing species and does not seem to

be influenced by the ancillary acetylide ligand. The TA experiments in the presence of excess DABCO gave similar results, since the positive charge localized on the Pt−acetylide framework is reductively quenched by the amine, and the origin of the resulting transient is essentially the $^{t}Bu_3tpy^{\bullet -}$ moiety. Thorough analysis of data collected from TA studies on the microsecond scale, reductive quenching of the excited state, and spectroelectrochemical experiments allow us to assert that the $^{t}Bu_3tpy$ radical anion formation in the CT excited state does not account for the intense TA features throughout the visible and NIR regions. The excited-state absorptions seem to be strongly tied to the photogenerated hole that is delocalized across the Pt center and the ancillary acetylide ligand. However, the instability of these complexes toward one-electron oxidation prohibits an exact assignment of whether the excited-state absorptions result from transitions localized in the photogenerated hole or whether they result from transitions between the intramolecular charge-separated species. Experiments that probe the optical transitions in the photogenerated hole will be necessary to unravel this dilemma. Work on related Pt(II) chromophores possessing stable one-electron oxidations is currently underway to resolve this issue.

Acknowledgment. The BGSU portion of the work was supported by the AFOSR (FA9550-05-1-0276), the NSF (CAREER Award CHE-0134782), the ACS-PRF (44138-AC3), and the BGSU Technology Innovation Enhancement Program. All TA measurements were performed in the Ohio Laboratory for Kinetic Spectrometry on the BGSU campus. The CNRS/ULP/ECPM and the ANR (FCP-OLEDs ANR-05-BLAN-0004-01) are acknowledged for partial financial support.

Supporting Information Available: Spectroelectrochemical measurements, additional transient-absorption spectra, electron-transfer quenching studies, and single-crystal X-ray analysis of **4**. This material is available free of charge via the Internet at http://pubs.acs.org.

IC0618652